

1
2
3
4
5
6
7
8
9
10
11
12
13

Observation-based variability in the global ocean carbon sink from 1959-2020

Val Bennington^{1,2}, Lucas Gloege³, Galen A. McKinley¹

¹Lamont-Doherty Earth Observatory at Columbia University
²Makai Ocean Engineering, Inc.
³NASA-GISS

Key Points:

- A temporal extension of an observation-based product for surface ocean pCO₂ (LDEO-HPD) is presented.
- An XGB algorithm adjusts ocean models toward in situ data for 1982-2020; a climatological adjustment is applied for 1959-1981.
- The ocean carbon sink from 1959-2020 has responded to atmospheric pCO₂ growth and volcanic eruptions.

Corresponding author: Val Bennington, Valerie.Bennington@makai.com

Abstract

The ocean plays a critical role in reducing the human impact on the climate by absorbing and sequestering CO₂. To quantify the ocean carbon sink, surface ocean pCO₂ must be estimated across space and time. Sparse in situ pCO₂ observations began in the 1980s, thus only global ocean biogeochemical models (GOBMs) have been the basis for quantification of the ocean carbon sink prior to the 1980s. The LDEO-Hybrid Physics Data product (LDEO-HPD) incorporates the physical knowledge within the GOBMs and corrects these estimates to observations. Here, we extend the LDEO-HPD product back to 1959 using a climatology of model-observation misfits. LDEO-HPD is closer to independent observations than unadjusted GOBMs. Most of the improvement from the GOBM prior in LDEO-HPD is attributable to the climatological adjustment, which supports the use of a climatological adjustment prior to 1982. Air-sea CO₂ fluxes for 1959-2020 demonstrate response to atmospheric pCO₂ growth and volcanic eruptions.

Plain Language Summary

The ocean removes carbon dioxide (CO₂) from the atmosphere and reduces climate change caused by humans. The magnitude of this removal can be estimated using computer models of ocean physics, chemistry, and biology, as well as statistical extrapolations of observations. The observational record is too sparse to directly reconstruct air-sea fluxes prior to 1982, but by combining models and a statistical approach, we make an estimate for 1959-present that is substantially informed by observations. The LDEO-HPD product for air-sea CO₂ exchange includes two periods, with the first previously published for 1982-2020 and the second being this extension back in time. For 1959 to 1981, LDEO-HPD corrects models using the average of data-based corrections derived from the observed period. The LDEO-HPD product agrees much better with independent observations than the models alone, and can be used to understand what controls year to year changes in the ocean carbon sink.

1 Introduction

By absorbing and sequestering carbon dioxide from the atmosphere, the global oceans play a critical role in modulating climate change. The ocean has absorbed 37% of fossil carbon emissions since the start of the industrial age (Friedlingstein et al., 2021). Quantifying the distribution of carbon emissions across the land biosphere, oceans, and atmosphere is an important support to climate policy (Peters et al., 2017). In order to estimate air-sea fluxes of carbon dioxide, the driver of these fluxes, the partial pressure of carbon dioxide in the surface waters (pCO₂), must be estimated.

Global ocean biogeochemical models (GOBMs) explicitly model the physics, biology and chemistry of the ocean carbonate system and resulting pCO₂. Observation-based products utilize sparse observations of the partial pressure of CO₂ (pCO₂) from the Surface Ocean CO₂ Atlas (SOCAT) (Bakker et al., 2016), and train a machine learning algorithm to relate these data to full-coverage observations of associate variables such that pCO₂ can be estimated at all points in space and time. Although the resulting statistical models often do not explicitly include the known physics of the ocean carbonate system, the results compare well to independent observations of pCO₂ (Gregor et al., 2019; Denvil-Sommer et al., 2019; Landschützer et al., 2014; Bennington et al., 2022). The mixed layer model of Rodenbeck et al. (2013, 2021) does incorporate some physical processes, differing from the other machine learning based products.

While both global ocean biogeochemical models (GOBMs) and observation-based products are used to estimate this air-sea gas exchange of CO₂ for the recent historical period, observation-based products have been limited to the period of in situ observations that began in the 1980s. Eight GOBMs were used to quantify the historical air-

Table 1. Global Ocean Biogeochemical Models (GOBMs) and their corresponding references.

Global ocean biogeochemical model	Reference
CESM-ETHZ	Doney et al. (2009)
FESCOM2-REcoM	Gurses et al. (2021)
MICOM-HAMOCC (NorESM1-OCv1.2)	Schwinger et al. (2016)
MOM6-COBALT (Princeton)	Adcroft et al. (2019)
MPIOM-HAMOCC6 (MPI)	Paulsen et al. (2017)
NEMO-PlankTOM5	Buitenhuis et al. (2013)
NEMO-PISCES (IPSL)	Aumont et al. (2015)
NEMO3.6-PISCESv2-gas (CNRM)	Berthet et al. (2019)

63 sea CO₂ flux prior to the 1980s in the Global Carbon Budget 2021 (Friedlingstein et al.,
 64 2021). To incorporate the physical knowledge contained within GOBMs, Gloege et al.
 65 (2022) utilized the machine-learning algorithm XGBoost (Chen & Guestrin, 2016) to learn
 66 model-observation misfits of simulated surface ocean pCO₂. The resulting data prod-
 67 uct (LDEO-HPD) showed an improved fit compared to the independent data over other
 68 data products. The resulting historical reconstruction of air-sea CO₂ fluxes from the ex-
 69 tended LDEO-HPD is within the range of other data products, and in agreement with
 70 2010-2020 mean flux estimates from the Global Carbon Budget 2021 (Friedlingstein et
 71 al., 2021).

72 LDEO-HPD estimated air-sea fluxes beginning in 1982. Here, we extend LDEO-
 73 HPD back in time by applying the climatology of 2000-2020 estimated GOBM-observation
 74 misfits to the GOBMs for 1959-1981. As discussed below, this approach is supported by
 75 the fact that much of the skill in LDEO-HPD against independent modern observations
 76 is due to the climatological correction.

77 This paper is organized as follows. We present the methods and resulting estimated
 78 air-sea CO₂ fluxes for 1959-2020. We then briefly examine the resulting estimated flux
 79 variability in four basins and globally.

80 2 Methods

81 The LDEO-HPD data product (Gloege et al., 2022) utilizes the nearly global cov-
 82 erage of satellite sea surface temperature (SST) (Reynolds et al., 2002), sea surface salin-
 83 ity (SSS) (Good et al., 2013), chlorophyll-a (Maritorena et al., 2010), geographic loca-
 84 tion, time of year, the climatology of mixed layer depth (de Boyer Montégut et al., 2004),
 85 and the machine learning algorithm XGBoost (Chen & Guestrin, 2016) to create a non-
 86 linear function between observations and the model-data misfit of surface ocean pCO₂.
 87 For the LDEO-HPD global reconstruction (1982-2020), misfits are calculated for each
 88 of eight (8) GOBMs to observed ocean surface pCO₂ (Bakker et al., 2016). Then, each
 89 of the GOBMs are independently adjusted with these corrections, which is unique to each
 90 GOBM. Finally, the average of the eight adjusted GOBMs is the final pCO₂ estimate.
 91 The GOBMs used here are the same as used in the Global Carbon Budget 2021 (Friedlingstein
 92 et al., 2021) (Table 1). The resulting model-data misfits are resolved at 1° latitude by
 93 1° longitude for each month. The complete description of the LDEO-HPD method and
 94 the resulting data product are detailed in Gloege et al. (2022).

95 2.1 Climatology of Model-Data Misfit

96 Given the lack of surface ocean pCO₂ observations prior to the 1980s, we must de-
 97 termine what corrections (model-data misfits) to apply to the models prior to 1982. Ex-

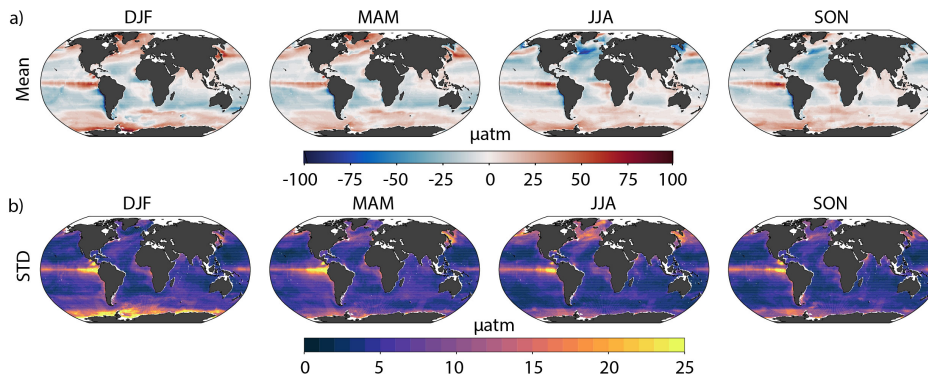


Figure 1. (a) Seasonal climatology (2000-2020) of model-data misfit in the Princeton model according to HPD. (b) Standard deviation of model-data misfit over 2000-2020 in the Princeton model, by season.

98 tending the analysis of climatological misfits by Gloege et al. (2022), we examine the in-
 99 terannual variability of the misfits for 2000-2020. We choose this period to best capture
 100 interannual variability (Bennington et al., 2022) since chlorophyll-a observations do not
 101 start until 1998 and a climatology of chlorophyll-a must be used prior (Landschützer et
 102 al., 2014).

103 The seasonal climatology and standard deviation of the model-data misfit for the
 104 Princeton GOBM is a representative example of the climatological misfit (Figure 1). Mean
 105 misfits are large in all seasons in the subpolar, equatorial, and Southern Ocean regions
 106 (Figure 1a). Interannual variability in the model-data misfit is quantified as the misfit
 107 standard deviation (Figure 1b). Year-to-year changes in misfits are significantly smaller
 108 in magnitude than the mean, typically less than $5 \mu\text{atm}$. Larger standard deviations can
 109 occur during the biologically productive seasons in the subpolar regions and Southern
 110 Ocean. The equatorial Pacific exhibits moderate interannual variability in all seasons.
 111 These patterns of misfit and variability are similar across most of the ocean models (Sup-
 112plementary), excepting MPIOM-HAMOCC (Gloege et al., 2022).

113 Since interannual variability in the reconstructed model-data misfit is generally small
 114 compared to the misfit mean, our approach to extending LDEO-HPD to the beginning
 115 of the model simulations is to use the monthly climatology of the 2000-2020 model-data
 116 misfit as the 1959-1981 correction for the GOBMs. This correction is separately calcu-
 117 lated for, and applied to, each of eight GOBMs. The final pCO_2 reconstruction is the
 118 ensemble mean of the eight corrected GOBM pCO_2 estimates (modeled pCO_2 + recon-
 119 structed correction).

Table 2. Observation-based products (Fay et al., 2021) and their corresponding references.

Data Product	Reference
LDEO-HPD	Gloege et al. (2022), this paper
JENA MLS	Rödenbeck et al. (2021)
CSIR ML6	Gregor et al. (2019)
MPI SOMFFN	Landschützer et al. (2014)
CMEMS FFNN	Denvil-Sommer et al. (2019)
pCO ₂ Residual	Bennington et al. (2022)

120 To assess how interannual variability is impacted by the climatological correction,
 121 comparison to independent data is required. These data do not exist in sufficient num-
 122 ber for the 1959-1981 period, but do exist after 1990. Thus, we create an alternative re-
 123 construction, $HPD_{ClimatologyTest}$, that applies the climatology of the model-data mis-
 124 fit for 2000-2020 to the entire reconstruction period (1959-2020). With $HPD_{ClimatologyTest}$,
 125 we can assess the impact of a climatological correction on the interannual variability of
 126 the reconstruction.

127 Figure 2 compares the original uncorrected GOBMs (squares), and five observation-
 128 based products (crosses) to GLODAP and LDEO observations for 1990-2020. The observation-
 129 based products all have substantially greater skill than the uncorrected GOBMs. $HPD_{ClimatologyTest}$
 130 (solid blue diamond) has similar skill as the suite of observation-based products (Fig-
 131 ure 2). This leads to an important finding, which is that most of LDEO-HPD’s skill is
 132 due to the correction of the GOBM’s climatological mean state and seasonality (Fay &
 133 McKinley, 2021) rather than their interannual variability. The additional skill achieved
 134 by adding interannual variability to the corrections (1) is shown by the difference between
 135 $HPD_{ClimatologyTest}$ and LDEO-HPD, which is modest for GLODAP (Figure 2a) and slightly
 136 larger for LDEO (Figure 2b). This additional increment of skill brings LDEO-HPD clos-
 137 est to the independent observations of these currently-available observation-based prod-
 138 ucts (Gloege et al., 2022).

139 2.2 CO₂ Flux Calculations

140 In the previous comparisons, we consider pCO₂. To assess the global ocean car-
 141 bon sink associated with these pCO₂ estimates, air-sea CO₂ exchange must be calculated.
 142 We use the same gas transfer velocity, solubility, winds, and ice for LDEO-HPD, other
 143 observation-based products, and the GOBMs so that differences in these calculations do
 144 not factor into the resulting comparison (Fay et al., 2021). EN4.2.2 salinity (Good et al.,
 145 2013); ERA5 winds, sea level pressure, and sea surface temperature; (Bell et al., 2020,
 146 2019); the wind scaling factor for ERA5 (Gregor & Fay, 2021); and Hadley sea ice frac-
 147 tional coverage (Rayner et al., 2003) are used. Unreconstructed coastal areas in data prod-
 148 ucts are filled with the scaled coastal pCO₂ climatology (Landschützer et al., 2020), also
 149 following Fay et al. (2021).

150 Air-sea CO₂ flux (FCO₂) is estimated using a bulk parameterization (Equation 1),

$$151 FCO_2 = K_w \cdot K_0 \cdot (1 - ice_{fraction}) \cdot (pCO_2^{sea} - pCO_2^{atm}) \quad (1)$$

152 where K_w is the gas-transfer velocity calculated from wind speeds, scaled to the 16.5 cm/hr
 153 14C bomb flux estimate according to Wanninkhof (1992) and Sweeney et al. (2007) as
 154 in Gregor and Fay (2021); K_0 is the solubility calculated using salinity and SST; pCO_2^{atm}
 155 is the water vapor corrected atmospheric partial pressure of CO₂ from CarboScope (Rödenbeck,
 156 2005); and pCO_2^{sea} is the surface ocean pCO₂.

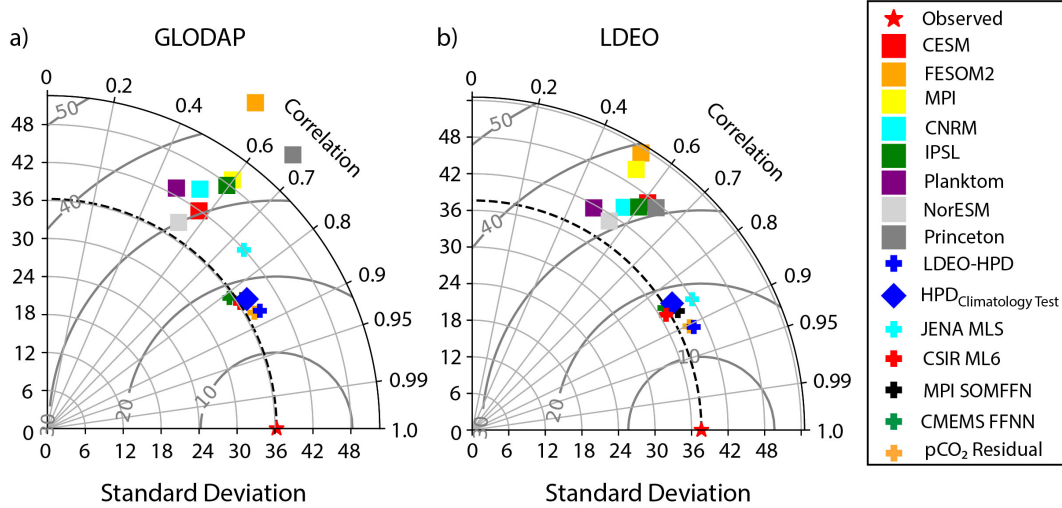


Figure 2. Taylor diagrams (Taylor, 2001) depict the skill of each ocean model (squares), previous data products (crosses), LDEO-HPD (blue cross), and $HPD_{ClimatologyTest}$. The ability to capture observed pCO_2 variability for 1990-2020 is evaluated against two global datasets (a) GLODAP and (b) LDEO. The red star indicates the standard deviation of each dataset. Distance along the radius represents the ability to capture observed variability (standard deviation). The distance along the circumference depicts correlation with the observations, and grey inlaid circles show unbiased RMSE compared to the observations.

157 Data products which incorporate observations of surface ocean pCO_2 include both
 158 natural and anthropogenic carbon in the resulting pCO_2 and CO_2 flux product. This
 159 is the net CO_2 flux ($F_{net} = F_{natural} + F_{ant}$). Global ocean biogeochemical models ex-
 160 clude the natural outgassing of riverine carbon ($F_{natural}$), which caused net CO_2 efflux
 161 from the preindustrial ocean (Aumont et al., 2001). To quantify the anthropogenic air-
 162 sea CO_2 flux, this $F_{natural}$ must be subtracted from our net flux, given that the mod-
 163 els have been corrected toward pCO_2 observations consistent with F_{net} . Quantifying the
 164 global air-sea CO_2 flux due to decomposition and outgassing of riverine carbon remains
 165 uncertain and is the topic of current research. Here, as in Gloege et al. (2022) and Bennington
 166 et al. (2022), we use an average of three estimates: Jacobson et al. (2007): (0.45 +/- 0.18
 167 PgC/yr), Resplandy et al. (2018): (0.78 +/- 0.41 PgC/yr), and Lacroix et al. (2020): (0.23
 168 Pg C / yr). The combined estimated efflux due to riverine carbon is 0.49 +/- 0.26 Pg
 169 C/yr, and we remove the efflux of 0.49 PgC/yr from the estimated annual air-sea CO_2
 170 fluxes calculated using the LDEO-HPD and other data products' pCO_2 .

171 **2.3 Box model**

172 The box model of McKinley et al. (2020) estimates the global-mean air-sea CO_2
 173 flux that occurs in response to the observed growth of atmospheric pCO_2 . It also has
 174 the option to include upper ocean heat content anomalies driven by the 3 most climat-
 175 ically impactful volcanic eruptions of the last 60 years: Agung in 1963, El Chichon in
 176 1982, and Mt Pinatubo in 1991 (Crisp et al., 2021). Comparing air-sea CO_2 fluxes es-
 177 timated by the box model for 1960-2019 allows consideration of flux variability with and
 178 without large volcanic influences and puts LDEO-HPD into context with previous com-
 179 parisons of the box model to observation-based products (McKinley et al., 2020).

3 Results

3.1 CO₂ Fluxes

Air-sea CO₂ fluxes for 1959-2020 from LDEO-HPD, the eight GOBMs, previously published observation-based products, and HPD_{ClimatologyTest} demonstrate a long-term increasing trend punctuated by interannual variability (Figure 3a). The most significant feature of this variability is the slowed growth in uptake during the 1990s (Le Quéré et al., 2007; Lovenduski et al., 2007, 2008; Fay & McKinley, 2013; Landschützer et al., 2015).

In LDEO-HPD, interannual variability prior to 1982 is driven by only the GOBMs; only the mean flux and seasonality have been adjusted with climatological model-data misfits. The adjustment leads to a larger mean flux than most of the GOBMs (Figure 3a). From 1982 onward, the flux in LDEO-HPD is very similar to HPD_{ClimatologyTest}, but has larger extremes. These differences are due to the interannually varying adjustments that are possible only during the observed period. This comparison indicates that LDEO-HPD likely underestimates the amplitude of interannual anomalies prior to 1982, which is to be expected when there are no data to directly drive the reconstruction toward extremes (Rödenbeck et al., 2021).

Examining the spatial patterns of the mean air-sea carbon dioxide fluxes for each 20 year period in Figure 3b, we see a reduced Pacific equatorial efflux during 1980-1999 compared to the other periods, consistent with the occurrence of multiple strong El Niño events in this period (e.g. 1982-83, 1997-98). In the Northern extratropics, the sink strengthens over time.

Integrated flux anomalies at each latitude reveal the spatial distribution of interannual anomalies (Figure 4). Consistent with the global timeseries (Figure 3a), the dominant feature is the long-term growth (red to blue) of the ocean carbon sink at all latitudes.

The Pacific Ocean has large integrated flux variability, with significant anomalies occurring on interannual timescales within the equatorial region as a result of ENSO (McKinley et al., 2004, 2017; Rödenbeck et al., 2021). The Southern Ocean experiences significant carbon sink decadal variations (Le Quéré et al., 2007; Lovenduski et al., 2007, 2008; Landschützer et al., 2015, 2016; Ritter et al., 2017; McKinley et al., 2017; Gruber et al., 2019). Significant negative anomalies (greater uptake) occur in the 1980s to early 1990s, with anomalies of greatest intensity in 1992-93. After 1997, a strong positive anomaly (reduced uptake) emerges and extends for about a decade. From 2009 on, the anomaly is again negative in the Southern Ocean. These decadal variations remain after detrending the air-sea fluxes (Figure S2). In the Atlantic, latitudes north of 40°N have the most intense fluxes. This basin is narrower than the others, and thus has a lower integrated flux and lower amplitude interannual variability. The Indian Ocean exhibits significant variability south of 10°S according to the reconstruction; however the region is particularly sparse in observations to guide the reconstruction, which should increase its uncertainty (Gloege et al., 2021).

Increased uptake occurs in the Pacific and Southern Oceans immediately following the eruptions of Agung (March 1963), El Chichon (March 1982) and Mt. Pinatubo (June 1991). These can also be seen in the detrended flux anomalies (Figure S2). In the equatorial Pacific, the El Niño events that tend to follow these eruptions drive significant flux anomalies (Eddebbbar et al., 2019). After El Chichon and Pinatubo, slight negative anomalies also occur in the Southern Hemisphere Atlantic. The globally-averaged box model of McKinley et al. (2020) parameterizes these eruptions as upper ocean heat content anomalies; the estimated fluxes correlate highly with LDEO-HPD (Figure S1d, $r=0.82$). If the eruptions are neglected, the correlation decreases ($r=0.64$). When both timeseries are detrended, the correlations remain significant only when the eruptions are

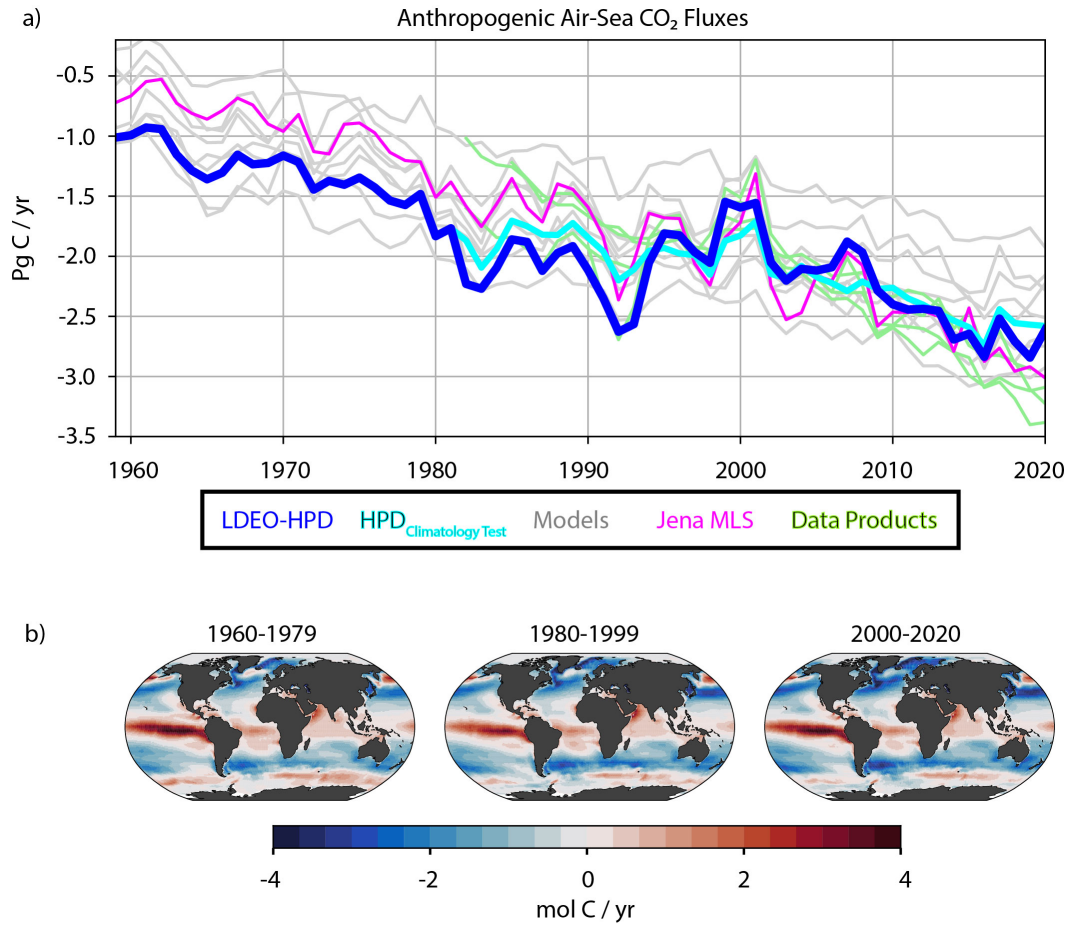


Figure 3. (a) Estimated air-sea CO₂ fluxes for 1959-2020 (Pg C/yr): LDEO-HPD (blue), HPD_{ClimatologyTest} (cyan), unadjusted GOBMs (grey), Jena MLS (magenta), other observation-based products (green); comparisons shown in separate panels in Figure S1. HPD_{ClimatologyTest} is identical to LDEO-HPD prior to 1982. (b) Map of mean air-sea CO₂ fluxes for 1960-1979, 1980-1999, and 2000-2020 according to LDEO-HPD (mol C / yr).

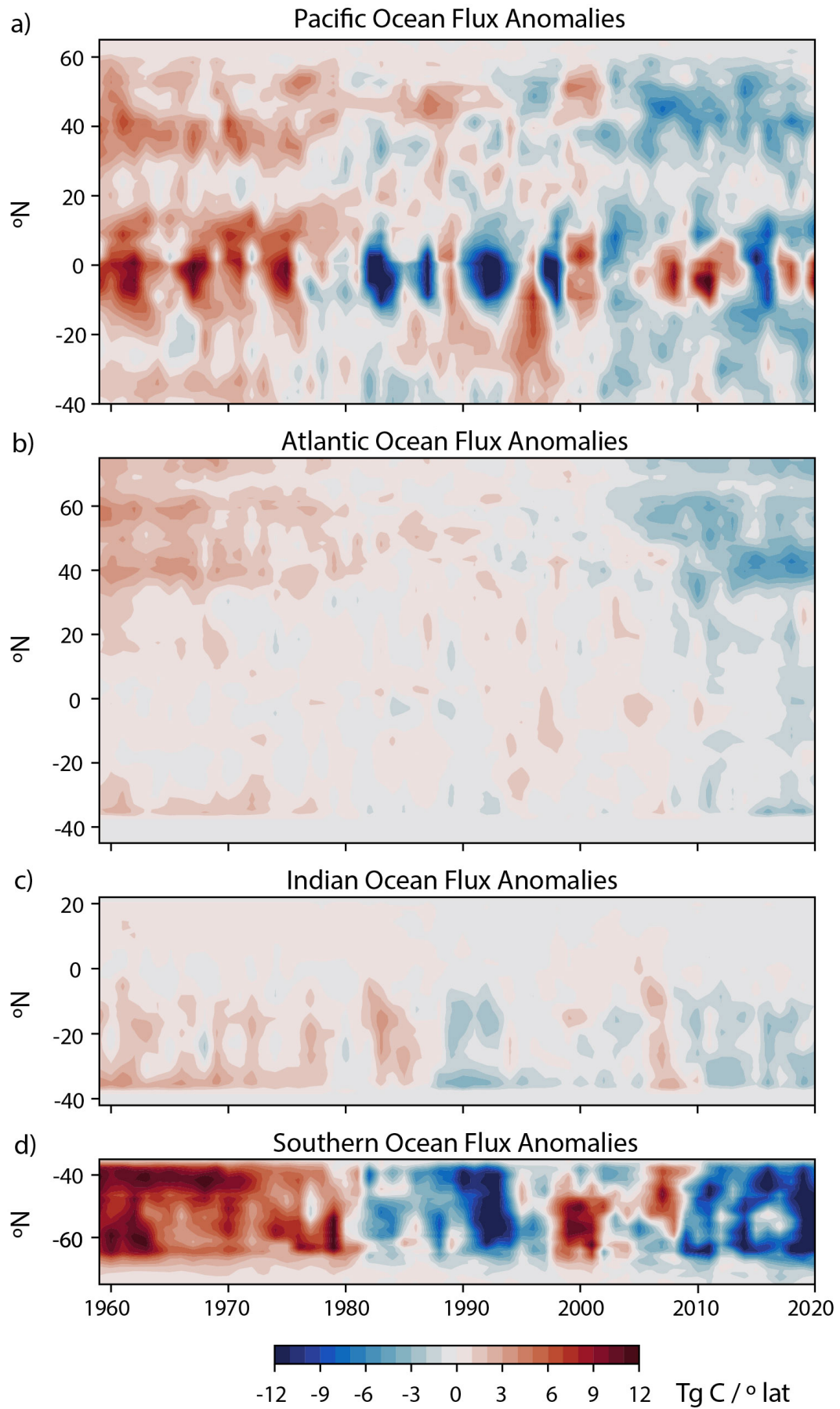


Figure 4. Air-sea CO₂ flux anomalies in four ocean basins (TgC/yr/°lat).

231 included in the box model (with eruptions, $r=0.51$, $p<0.05$; without, $r=-0.23$, $p=0.13$).
232 Thus, both the box model and the spatial patterns of flux anomalies (Figure 4) indicates
233 the potential for large volcanoes to impact interannual variability of the global ocean car-
234 bon sink since 1959. A more detailed study of this issue in the LDEO-HPD product will
235 be presented elsewhere.

236 4 Discussion and Conclusions

237 This work temporally extends the LDEO-HPD data product back in time to be-
238 gin in 1959. For 1982-2020, model-data misfits are calculated for each model and each
239 month as in Gloege et al. (2022). For 1959-1981, the monthly climatology of this cor-
240 rection for 2000-2020 is applied independently to each of eight GOBMs. Across all years,
241 the final LDEO-HPD $p\text{CO}_2$ estimate is the average across the eight corrected models.

242 In comparison to independent data in the modern era, we find that the substan-
243 tial improvement over uncorrected GOBMs is due primarily to the correction of the model
244 mean and seasonality; i.e. the climatological correction. There are significant regional
245 biases in the mean and seasonality of many GOBMs (Fay & McKinley, 2021; Hauck et
246 al., 2020), and this observation-based approach can substantially improve these biases
247 to bring the resulting estimates closer to observations (Figure 2). At the same time, this
248 approach can preserve the GOBMs capability to represent interannual variability (Fig-
249 ure 3) that occurs in response to external forcing and internal ocean processes. By com-
250 bining the strengths of models and observations with the LDEO-HPD approach, we have
251 developed a robust approach to temporally extend this observation-based product back
252 to 1959.

253 Compared to another recently developed extension, Jena MLS (Rödenbeck et al.,
254 2021), the two sink estimates are significantly correlated ($r=0.93$, $p=0$ and $r=0.66$, $p=0$
255 when series are detrended). The two reconstructions span the range of model flux es-
256 timates prior to 1990s (Figure 3b), after which observations better constrain the prod-
257 ucts. Jena-MLS has a significantly larger estimated trend in the ocean carbon sink over
258 the reconstructed period. However, as discussed by Rödenbeck et al. (2021) (their sec-
259 tion A2), Jena-MLS in its current version overestimates the flux trend; thus, it likely un-
260 derestimates the sink for the pre-observation decades.

261 LDEO-HPD indicates that the ocean carbon sink increased over the last 60 years,
262 due to the long-term growth of atmospheric $p\text{CO}_2$ (Raupach et al., 2014; McKinley et
263 al., 2020; Ridge & McKinley, 2021). Long-term growth is punctuated by year-to-year vari-
264 ability. Consistent with many earlier studies, the equatorial Pacific and Southern Ocean
265 have the largest integrated impact on variations of the sink (Le Quéré et al., 2003; McKin-
266 ley et al., 2004; Resplandy et al., 2015; McKinley et al., 2017; Landschützer et al., 2016;
267 Hauck et al., 2020). The timing of these changes is consistent with ENSO variability in
268 the equatorial Pacific. The Southern Ocean exhibits strong decadal timescale variations
269 for which both internal and externally-forced mechanisms have been proposed. Better
270 understanding the variability of ocean carbon uptake in the Southern Ocean and across
271 the globe is an important task that can be facilitated by observation-based products such
272 as LDEO-HPD.

Acknowledgments

The authors acknowledge support from NOAA (NA20OAR4310340) and the Data Science Institute of Columbia University. L.G was sponsored by the National Aeronautics and Space Administration (NASA) through a contract with ORAU. The views and conclusions contained in this document are those of the authors and should not be interpreted as representing the official policies, either expressed or implied, of the National Aeronautics and Space Administration (NASA) or the U.S. Government. The U.S. Government is authorized to reproduce and distribute reprints for Government purposes notwithstanding any copyright notation herein. We acknowledge that all data providers and quality controllers who work tirelessly to maintain the SOCAT database. We also acknowledge the ocean biogeochemical modelers who contribute to the Global Carbon Budget for sharing their output with us; and we thank J. Hauck specifically for her leadership on this effort. EN.4.2.2 data were obtained from <https://www.metoffice.gov.uk/hadobs/en4/> and are © British Crown Copyright, Met Office, [2022], provided under a Non-Commercial Government Licence:

<http://www.nationalarchives.gov.uk/doc/non-commercial-government-licence/version/2/>.

Project code available at: https://github.com/valbennington/LDE0_HPD_extension.

References

- Adcroft, A., Anderson, W., Balaji, V., Blanton, C., Bushuk, M., Dufour, C. O., ... Zhang, R. (2019). The GFDL Global Ocean and Sea Ice Model OM4.0: Model description and simulation features. *Journal of Advances in Modeling Earth Systems*, *11*(10), 3167-3211. doi: <https://doi.org/10.1029/2019MS001726>
- Aumont, O., Ethé, C., Tagliabue, A., Bopp, L., & Gehlen, M. (2015). PISCES-v2: An ocean biogeochemical model for carbon and ecosystem studies. *Geoscientific Model Development*, *8*, 2465–2513. doi: 10.5194/gmd-8-2465-2015
- Aumont, O., Orr, J. C., Monfray, P., Ludwig, W., Amiotte-Suchet, P., & Probst, J.-L. (2001). Riverine-driven interhemispheric transport of carbon. *Global Biogeochemical Cycles*, *15*(2), 393-405. doi: <https://doi.org/10.1029/1999GB001238>
- Bakker, D. C. E., Pfeil, B., Landa, C. S., Metzl, N., O'Brien, K. M., Olsen, A., ... Xu, S. (2016). A multi-decade record of high-quality $f\text{CO}_2$ data in version 3 of the Surface Ocean CO_2 Atlas (SOCAT). *Earth System Science Data*, *8*(2), 383–413. doi: 10.5194/essd-8-383-2016
- Bell, B., Hersbach, H., Berrisford, P., Dahlgren, P., Horányi, A., Muñoz Sabater, J., ... Thépaut, J.-N. (2019). *ERA5 monthly averaged data on single levels from 1979 to present*. Copernicus Climate Change Service (C3S) Climate Data Store (CDS). doi: 10.24381/cds.f17050d7
- Bell, B., Hersbach, H., Berrisford, P., Dahlgren, P., Horányi, A., Muñoz Sabater, J., ... Thépaut, J.-N. (2020). *ERA5 monthly averaged data on single levels from 1950 to 1978 (preliminary version)*. Copernicus Climate Change Service (C3S) Climate Data Store (CDS).
- Bennington, V., Galjanic, T., & McKinley, G. A. (2022). Estimating historical air-sea CO_2 fluxes: Incorporating physical knowledge within a data-only approach. *Journal of Advances in Modeling Earth Systems, In Review*. Retrieved from <https://doi.org/10.1002/essoar.10510196.1>
- Berthet, S., Séférian, R., Bricaud, C., Chevallier, M., Voltaire, A., & Ethé, C. (2019). Evaluation of an online grid-coarsening algorithm in a global eddy-admitting ocean biogeochemical model. *Journal of Advances in Modeling Earth Systems*, *11*(6), 1759-1783. doi: <https://doi.org/10.1029/2019MS001644>
- Buitenhuis, E. T., Hashioka, T., & Quéré, C. L. (2013). Combined constraints on global ocean primary production using observations and models. *Global Biogeochemical Cycles*, *27*(3), 847-858. doi: <https://doi.org/10.1002/gbc.20074>
- Chen, T., & Guestrin, C. (2016). Xgboost: A scalable tree boosting system. *CoRR*,

- 326 *abs/1603.02754*.
- 327 Crisp, D., Dolman, H., Tanhua, T., McKinley, G. A., Hauck, J., Eggleston, S., &
328 Aich, V. (2021). How well do we understand the land-ocean-atmosphere carbon
329 cycle? *Reviews in Geophysics, in review*. doi: 10.1002/essoar.10506293.2
- 330 de Boyer Montégut, C., Madec, G., Fischer, A. S., Lazar, A., & Iudicone, D. (2004).
331 Mixed layer depth over the global ocean: An examination of profile data and a
332 profile-based climatology. *Journal of Geophysical Research: Oceans*, 109(C12).
333 doi: <https://doi.org/10.1029/2004JC002378>
- 334 Denvil-Sommer, A., Gehlen, M., Vrac, M., & Mejia, C. (2019). LSCE-FFNN-v1: a
335 two-step neural network model for the reconstruction of surface ocean pCO₂
336 over the global ocean. *Geoscientific Model Development*, 12, 2091–2105. doi:
337 <https://doi.org/10.5194/gmd-12-2091-2019>
- 338 Doney, S. C., Lima, I., Feely, R. A., Glover, D. M., Lindsay, K., Mahowald, N., ...
339 Wanninkhof, R. (2009). Mechanisms governing interannual variability in
340 upper-ocean inorganic carbon system and air-sea CO₂ fluxes: Physical climate
341 and atmospheric dust. *Deep Sea Research Part II: Topical Studies in Oceanog-*
342 *raphy*, 56(8), 640-655. doi: <https://doi.org/10.1016/j.dsr2.2008.12.006>
- 343 Eddelbar, Y. A., Rodgers, K. B., Long, M. C., Subramanian, A. C., Xie, S.-P., &
344 Keeling, R. F. (2019). El niño-like physical and biogeochemical ocean re-
345 sponse to tropical eruptions. *Journal of Climate*, 32(9), 2627 - 2649. doi:
346 10.1175/JCLI-D-18-0458.1
- 347 Fay, A. R., Gregor, L., Landschützer, P., McKinley, G. A., Gruber, N., Gehlen, M.,
348 ... Zeng, J. (2021). SeaFlux: harmonization of air-sea CO₂ fluxes from sur-
349 face pCO₂ data products using a standardized approach. *Earth System Science*
350 *Data*, 13(10), 4693–4710. doi: 10.5194/essd-13-4693-2021
- 351 Fay, A. R., & McKinley, G. A. (2013). Global trends in surface ocean pCO₂ from in
352 situ data. *Global Biogeochemical Cycles*, 27(2), 541–557.
- 353 Fay, A. R., & McKinley, G. A. (2021). Observed regional fluxes to constrain mod-
354 eled estimates of the ocean carbon sink. *Geophysical Research Letters*, 48(20),
355 e2021GL095325.
- 356 Friedlingstein, P., Jones, M. W., O’Sullivan, M., Andrew, R. M., Bakker, D. C.,
357 Hauck, J., ... others (2021). Global carbon budget 2021. *Earth System*
358 *Science Data Discussions*, 1–191.
- 359 Gloege, L., McKinley, G. A., Landschützer, P., Fay, A. R., Frölicher, T. L., Fyfe,
360 J. C., ... Takano, Y. (2021). Quantifying errors in observationally based es-
361 timates of ocean carbon sink variability. *Global Biogeochemical Cycles*, 35(4),
362 e2020GB006788. doi: <https://doi.org/10.1029/2020GB006788>
- 363 Gloege, L., Yan, M., Zheng, T., & McKinley, G. A. (2022). Improved quantifica-
364 tion of ocean carbon uptake by using machine learning to merge global models
365 and pCO₂ data. *Journal of Advances in Modeling Earth Systems*, 14. doi:
366 10.1029/2021ms002620
- 367 Good, S. A., Martin, M. J., & Rayner, N. A. (2013). EN4: Quality controlled
368 ocean temperature and salinity profiles and monthly objective analyses with
369 uncertainty estimates. *Journal of Geophysical Research: Oceans*, 118(12),
370 6704-6716. doi: <https://doi.org/10.1002/2013JC009067>
- 371 Gregor, L., & Fay, A. (2021). *SeaFlux: harmonised sea-air CO2 fluxes from sur-*
372 *face pCO2 data products using a standardised approach*. Zenodo. doi: 10.5281/
373 zenodo.5482547
- 374 Gregor, L., Lebehot, A. D., Kok, S., & Monteiro, P. M. S. (2019). A com-
375 parative assessment of the uncertainties of global surface ocean CO₂ esti-
376 mates using a machine-learning ensemble (CSIR-ML6 version 2019a) – have
377 we hit the wall? *Geoscientific Model Development*, 12, 5113–5136. doi:
378 <https://doi.org/10.5194/gmd-12-5113-2019>
- 379 Gruber, N., Landschützer, P., & Lovenduski, N. S. (2019). The variable southern
380 ocean carbon sink. *Annual Review of Marine Science*, 11(1), 159-186. doi: 10

- 381 .1146/annurev-marine-121916-063407
- 382 Gurses, O., Hauck, J., Zeising, M., & Oziel, L. (2021). Global ocean biogeochemical
383 modelling with FESOM2-REcoM. In *EGU General Assembly Conference Ab-*
384 *stracts* (pp. EGU21–14980).
- 385 Hauck, J., Zeising, M., Le Quéré, C., Gruber, N., Bakker, D. C. E., Bopp, L., ...
386 Séférian, R. (2020). Consistency and challenges in the ocean carbon sink
387 estimate for the global carbon budget. *Frontiers in Marine Science*(7). doi:
388 10.3389/fmars.2020.571720
- 389 Jacobson, A. R., Mikaloff Fletcher, S. E., Gruber, N., Sarmiento, J. L., & Gloor, M.
390 (2007). A joint atmosphere-ocean inversion for surface fluxes of carbon dioxide:
391 1. methods and global-scale fluxes. *Global Biogeochemical Cycles*, 21(1). doi:
392 https://doi.org/10.1029/2005GB002556
- 393 Lacroix, F., Ilyina, T., & Hartmann, J. (2020). Oceanic CO₂ outgassing and biolog-
394 ical production hotspots induced by pre-industrial river loads of nutrients and
395 carbon in a global modeling approach. *Biogeosciences*, 17(1), 55-88.
- 396 Landschützer, P., Gruber, N., & Bakker, D. C. E. (2016). Decadal variations and
397 trends of the global ocean carbon sink. *Global Biogeochemical Cycles*, 30(10),
398 1396-1417. doi: https://doi.org/10.1002/2015GB005359
- 399 Landschützer, P., Gruber, N., Bakker, D. C. E., & Schuster, U. (2014). Recent vari-
400 ability of the global ocean carbon sink. *Global Biogeochemical Cycles*, 28(9),
401 927-949. doi: https://doi.org/10.1002/2014GB004853
- 402 Landschützer, P., Gruber, N., Haumann, F. A., Rödenbeck, C., Bakker, D. C. E.,
403 van Heuven, S., ... Wanninkhof, R. (2015). The reinvigoration of
404 the southern ocean carbon sink. *Science*, 349(6253), 1221-1224. doi:
405 10.1126/science.aab2620
- 406 Landschützer, P., Laruelle, G. G., Roobaert, A., & Regnier, P. (2020). A uniform
407 pCO₂ climatology combining open and coastal oceans. *Earth System Science*
408 *Data*, 12(4), 2537-2553.
- 409 Le Quéré, C., Aumont, O., Monfray, P., & Orr, J. (2003). Propagation of climatic
410 events on ocean stratification, marine biology, and CO₂: Case studies over the
411 1979–1999 period. *Journal of Geophysical Research: Oceans*, 108(C12).
- 412 Le Quéré, C., Rödenbeck, C., Buitenhuis, E. T., Conway, T. J., Langenfelds, R.,
413 Gomez, A., ... others (2007). Saturation of the Southern Ocean CO₂ sink due
414 to recent climate change. *Science*, 316(5832), 1735–1738.
- 415 Lovenduski, N., Gruber, N., & Doney, S. C. (2008). Toward a mechanistic under-
416 standing of the decadal trends in the Southern Ocean carbon sink. *Global Bio-*
417 *geochemical Cycles*, 22, GB3016.
- 418 Lovenduski, N., Gruber, N., Doney, S. C., & Lima, I. D. (2007). Enhanced CO₂ out-
419 gassing in the Southern Ocean from a positive phase of the Southern Annular
420 Mode. *Global Biogeochemical Cycles*, 21(2), GB2026.
- 421 Maritorena, S., d'Andon, O. H. F., Mangin, A., & Siegel, D. A. (2010). Merged
422 satellite ocean color data products using a bio-optical model: Characteristics,
423 benefits and issues. *Remote Sensing of Environment*, 114(8), 1791-1804. doi:
424 https://doi.org/10.1016/j.rse.2010.04.002
- 425 McKinley, G. A., Fay, A. R., Eddebbbar, Y. A., Gloege, L., & Lovenduski, N. S.
426 (2020). External forcing explains recent decadal variability of the ocean carbon
427 sink. *AGU Advances*, 1(2), e2019AV000149. doi: https://doi.org/10.1029/
428 2019AV000149
- 429 McKinley, G. A., Fay, A. R., Lovenduski, N. S., & Pilcher, D. J. (2017). Natural
430 variability and anthropogenic trends in the ocean carbon sink. *Annual review*
431 *of marine science*, 9, 125–150.
- 432 McKinley, G. A., Follows, M. J., & Marshall, J. (2004). Mechanisms of air-sea CO₂
433 flux variability in the equatorial Pacific and the North Atlantic. *Global Biogeo-*
434 *chemical Cycles*, 18(2).
- 435 Paulsen, H., Ilyina, T., Six, K. D., & Stemmler, I. (2017). Incorporating a prognostic

- 436 representation of marine nitrogen fixers into the global ocean biogeochemical
 437 model HAMOCC. *Journal of Advances in Modeling Earth Systems*, 9(1), 438 -
 438 464.
- 439 Peters, G. P., Quéré, C. L., Andrew, R. M., Canadell, J. G., Friedlingstein, P., Ily-
 440 ina, T., ... Tans, P. (2017). Towards real-time verification of CO₂ emissions.
 441 *Nature Climate Change*, 7(12), 848-850.
- 442 Raupach, M. R., Davis, S. J., Peters, G. P., Andrew, R. M., Canadell, J. G., Ciais,
 443 P., ... Le Quere, C. (2014). Sharing a quota on cumulative carbon emissions.
 444 *Nature Climate Change*, 4(10), 873-879.
- 445 Rayner, N. A., Parker, D. E., Horton, E. B., Folland, C. K., Alexander, L. V., Row-
 446 ell, D. P., ... Kaplan, A. (2003). Global analyses of sea surface temper-
 447 ature, sea ice, and night marine air temperature since the late nineteenth
 448 century. *Journal of Geophysical Research: Atmospheres*, 108(D14). doi:
 449 <https://doi.org/10.1029/2002JD002670>
- 450 Resplandy, L., Keeling, R. F., Rödenbeck, C., Stephens, B. B., Khatiwala, S.,
 451 Rodgers, K. B., ... Tans, P. P. (2018). Revision of global carbon fluxes
 452 based on a reassessment of oceanic and riverine carbon transport. *Nature*
 453 *Geoscience*, 11(7), 504-509.
- 454 Resplandy, L., Séférian, R., & Bopp, L. (2015). Natural variability of CO₂ and O₂
 455 fluxes: What can we learn from centuries-long climate models simulations?
 456 *Journal of Geophysical Research: Oceans*, 120(1), 384-404.
- 457 Reynolds, R. W., Rayner, N. A., Smith, T. M., Stokes, D. C., & Wang, W. (2002).
 458 An improved in situ and satellite SST analysis for climate. *Journal of Climate*,
 459 15(13), 1609-1625.
- 460 Ridge, S. M., & McKinley, G. A. (2021). Ocean carbon uptake under aggressive
 461 emission mitigation. *Biogeosciences*, 18(8), 2711-2725.
- 462 Ritter, R., Landschützer, P., Gruber, N., Fay, A., Iida, Y., Jones, S., ... others
 463 (2017). Observation-based trends of the Southern Ocean carbon sink. *Geophys-
 464 ical Research Letters*, 44(24), 12-339.
- 465 Rödenbeck, C., DeVries, T., Hauck, J., Le Quéré, C., & Keeling, R. (2021). Data-
 466 based estimates of interannual sea-air CO₂ flux variations 1957-2020 and their
 467 relation to environmental drivers. *Biogeosciences Discussions*, 2021, 1-43. doi:
 468 10.5194/bg-2021-304
- 469 Rödenbeck, C. (2005). *Estimating CO₂ sources and sinks from atmospheric mixing
 470 ratio measurements using a global inversion of atmospheric transport* (Tech.
 471 Rep. No. 6). Max Planck Institute for Biogeochemistry, Jena. Retrieved from
 472 <http://www.bgc-jena.mpg.de/CarboScope/>
- 473 Rödenbeck, C., Keeling, R. F., Bakker, D. C. E., Metzl, N., Olsen, A., Sabine, C., &
 474 Heimann, M. (2013). Global surface-ocean pCO₂ and sea-air CO₂ flux variabil-
 475 ity from an observation-driven ocean mixed-layer scheme. *Ocean Science*, 9(2),
 476 193 - 216.
- 477 Schwinger, J., Goris, N., Tjiputra, J. F., Kriest, I., Bentsen, M., Bethke, I., ...
 478 Heinze, C. (2016). Evaluation of NorESM-OC (versions 1 and 1.2), the
 479 ocean carbon-cycle stand-alone configuration of the Norwegian Earth System
 480 Model (NorESM1). *Geoscientific Model Development*, 9(8), 2589-2622. doi:
 481 10.5194/gmd-9-2589-2016
- 482 Sweeney, C., Gloor, E., Jacobson, A. R., Key, R. M., McKinley, G., Sarmiento, J. L.,
 483 & Wanninkhof, R. (2007). Constraining global air-sea gas exchange for CO₂
 484 with recent bomb 14C measurements. *Global Biogeochemical Cycles*, 21(2).
- 485 Taylor, K. E. (2001). Summarizing multiple aspects of model performance in a single
 486 diagram. *Journal of Geophysical Research: Atmospheres*, 106(D7), 7183-7192.
 487 doi: <https://doi.org/10.1029/2000JD900719>
- 488 Wanninkhof, R. (1992). Relationship between wind speed and gas exchange over
 489 the ocean. *Journal of Geophysical Research: Oceans*, 97(C5), 7373-7382. doi:
 490 <https://doi.org/10.1029/92JC00188>